

“Selective inhibitors of *H. pylori* methylthioadenosine nucleosidase and human methylthioadenosine phosphorylase”

Rajesh K. Harijan, Oskar Hoff, Rodrigo G. Ducati, Ross S. Firestone,
Brett M. Hirsch, Gary B. Evans, Vern L. Schramm, and Peter C. Tyler

J. Med. Chem., **Just Accepted Manuscript** • DOI: 10.1021/acs.jmedchem.8b01642 • Publication Date (Web): 12 Mar 2019

Downloaded from <http://pubs.acs.org> on March 13, 2019

Just Accepted

“Just Accepted” manuscripts have been peer-reviewed and accepted for publication. They are posted online prior to technical editing, formatting for publication and author proofing. The American Chemical Society provides “Just Accepted” as a service to the research community to expedite the dissemination of scientific material as soon as possible after acceptance. “Just Accepted” manuscripts appear in full in PDF format accompanied by an HTML abstract. “Just Accepted” manuscripts have been fully peer reviewed, but should not be considered the official version of record. They are citable by the Digital Object Identifier (DOI®). “Just Accepted” is an optional service offered to authors. Therefore, the “Just Accepted” Web site may not include all articles that will be published in the journal. After a manuscript is technically edited and formatted, it will be removed from the “Just Accepted” Web site and published as an ASAP article. Note that technical editing may introduce minor changes to the manuscript text and/or graphics which could affect content, and all legal disclaimers and ethical guidelines that apply to the journal pertain. ACS cannot be held responsible for errors or consequences arising from the use of information contained in these “Just Accepted” manuscripts.



1
2
3
4
5 **Selective inhibitors of *H. pylori* methylthioadenosine nucleosidase and human**
6 **methylthioadenosine phosphorylase**
7
8
9

10
11 Rajesh K. Harijan^a, Oskar Hoff^b, Rodrigo G. Ducati^a, Ross S. Firestone^a, Brett M. Hirsch^a, Gary
12 B. Evans^b, Vern L. Schramm^{a,*} and Peter C. Tyler^{b,*}
13
14
15

16
17 ^a Department of Biochemistry, Albert Einstein College of Medicine, New York 10461, USA.
18

19
20 ^b Ferrier Research Institute, Victoria University of Wellington, Wellington 5040, New Zealand.
21
22

23
24 * Corresponding authors: vern.schramm@einstein.yu.edu or peter.tyler@vuw.ac.nz
25
26

27
28 **KEYWORDS:** transition-state analogue; futasine pathway; menaquinone; immucillins; S-
29 adenosylmethionine.
30
31

32
33
34
35 **ABBREVIATIONS:**
36

37
38 MTDIA: methylthio-DADMe-Immucillin-A; MTA: S-methyl-5'-thioadenosine; All: allyl; DQF-
39 COSY: double-quantum filtered correlation spectroscopy; Q-TOF: quadrupole time-of-flight;
40
41 MTAN: 5'-methylthioadenosine/S-adenosylhomocysteine nucleosidase; *Hp*MTAN: *Helicobacter*
42 *pylori* MTAN; MTAP: 5'-methylthioadenosine phosphorylase; MTR: 5-methylthio- α -D-ribose 1-
43 phosphate; SAM: S-Adenosylmethionine; SAH: S-adenosylhomocysteine, SRH: S-
44 ribosylhomocysteine
45
46
47
48
49
50
51
52
53
54
55
56
57
58
59
60

ABSTRACT

Bacterial 5'-methylthioadenosine/S-adenosylhomocysteine nucleosidase (MTAN) hydrolyzes adenine from its substrates to form S-methyl-5'-thioribose and S-ribosyl-L-homocysteine. MTANs are involved in quorum sensing, menaquinone synthesis and 5'-methylthioadenosine recycling to S-adenosylmethionine. *Helicobacter pylori* uses MTAN in its unusual menaquinone pathway, making *H. pylori* MTAN a target for antibiotic development. Human 5'-methylthioadenosine phosphorylase (MTAP), a reported anticancer target, catalyzes phosphorolysis of 5'-methylthioadenosine to salvage S-adenosylmethionine. Transition-state analogues designed for *Hp*MTAN and MTAP show significant overlap in specificity. Fifteen unique transition-state analogues are described here and are used to explore inhibitor specificity. Several analogues of *Hp*MTAN bind in the picomolar range while inhibiting human MTAP with orders of magnitude weaker affinity. Structural analysis of *Hp*MTAN shows inhibitors extending through a hydrophobic channel to the protein surface. The more enclosed catalytic sites of human MTAP require the inhibitors to adopt a folded structure, displacing the phosphate nucleophile from the catalytic site.

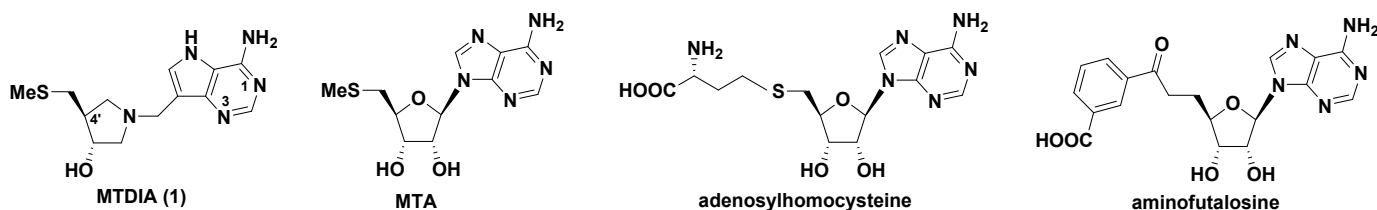
INTRODUCTION

S-Adenosylmethionine (SAM) is involved in biological methylation reactions, in polyamine biosynthesis and as a precursor of glutathione.^{1,2} Two molecules of 5'-methylthioadenosine (MTA) are formed from SAM in the synthesis of each spermine molecule (Scheme 1). In humans, MTA is metabolized only by methylthioadenosine phosphorylase (MTAP) to form 5-methylthio- α -D-ribose 1-phosphate (MTR) and adenine. These are precursors for methionine and ATP which can be recycled to SAM (Figure 1).^{3,4} Inhibition of MTAP in mammals causes elevated MTA and decreased recycling of MTA to SAM.^{5,6} Synthetic-lethal genetic analysis of MTAP-deleted cancer cell lines indicate sensitivity of these cell lines to pathways related to SAM-related methyl transfer.⁷⁻¹⁰ It has also been proposed that inhibitors of MTAP may have anti-cancer applications alone or in drug combinations, as they demonstrate anti-cancer properties in mouse xenograft models.^{5,6}

Most bacteria express methylthioadenosine/*S*-adenosylhomocysteine nucleosidase (MTAN) instead of MTAP. The enzyme hydrolyzes MTA and *S*-adenosylhomocysteine (SAH) to MTR or *S*-ribosylhomocysteine (SRH) and adenine, respectively (Scheme 1, Figure 1). The MTAN reaction product, SRH, is used in the biosynthesis of homoserine lactones to form AI-2 quorum sensing molecules.¹¹⁻¹³ MTAN is not essential in most bacteria, but a few species use the unusual futasine pathway for the biosynthesis of menaquinone, where MTAN plays an essential role.^{14,15} These organisms include the pathogens *Helicobacter pylori* and *Campylobacter jejuni*. Inhibition of this pathway is reported to be lethal to *H. pylori*.^{16,17} Inhibitors of MTAN are also expected to reduce polyamine biosynthesis and block production of quorum sensing autoinducer (AI-2) molecules. For these reasons, human MTAP and bacterial MTAN enzymes are of interest as drug targets.

1
2
3
4
5
6
7
8
9
10
11
12
13
14
15
16
17
18
19
20
21
22
23
24
25
26
27
28
29
30
31
32
33
34
35
36
37
38
39
40
41
42
43
44
45
46
47
48
49
50
51
52
53
54
55
56
57
58
59
60

Transition-state analogue enzyme inhibitors have the potential to bind orders of magnitude more tightly than substrates. Studies focused on *N*-ribosyltransferases have identified transition states with ribocation character.¹⁸ MTAP and MTAN share MTA as a substrate and form similar transition states, leading to similar interactions with transition-state analogues (Figure 1).¹⁹⁻²¹ MTAP inhibitors have shown efficacy in animal models against human tumors, while MTAN inhibitors influence bacterial quorum sensing and are antibiotics in organisms using the futasine pathway of menaquinone synthesis, notably, *H. pylori*. We have reported transition-state analogues as inhibitors of human MTAP and several bacterial MTAN enzymes.¹⁶⁻²⁶ Of several inhibitory chemical scaffolds, the DADMe-Immucillin structure exemplified by MTDIA (**1**) is optimal for these enzymes (Scheme 1). Both enzymes tolerate substituents in the 4'-position of the 3'-hydroxypyrrolidine ring – in particular for the bacterial MTAN enzymes. Here we report new analogues to explore the structure-activity relationships for human MTAP and *Hp*MTAN.



Scheme 1.

The transition-state structures of MTAN and MTAP enzymes have been solved by kinetic isotope effect measurements and quantum chemical calculations.^{19,21,27,28} Transition-state analogues for these enzymes act as strong catalytic-site inhibitors of the enzyme.²⁴⁻²⁶ Two inhibitors in particular, methylthio-DADMe-Immucillin-A (MTDIA) and *parachloro*-phenylthio-DADMe-Immucillin-A (*p*Cl-PhT-DADMe-ImmA), were slow-onset inhibitors with dissociation

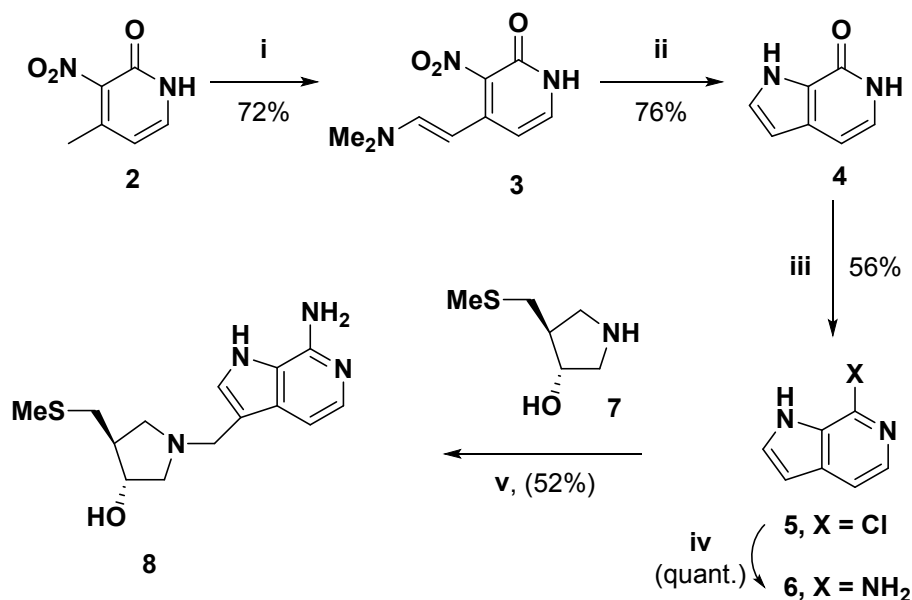
constants (K_i^*) of 86 pM and 10 pM, respectively for human MTAP, and 86 and 570 pM, respectively for *Hp*MTAN.^{17,22} Inhibitors reported here provide insight into the 4'-substituent inhibitor specificity for transition-state analogues of *Hp*MTAN and human MTAP.

RESULTS AND DISCUSSION

Synthesis of new transition-state analogue inhibitors

Modifications in the 9-deazaadenine moiety

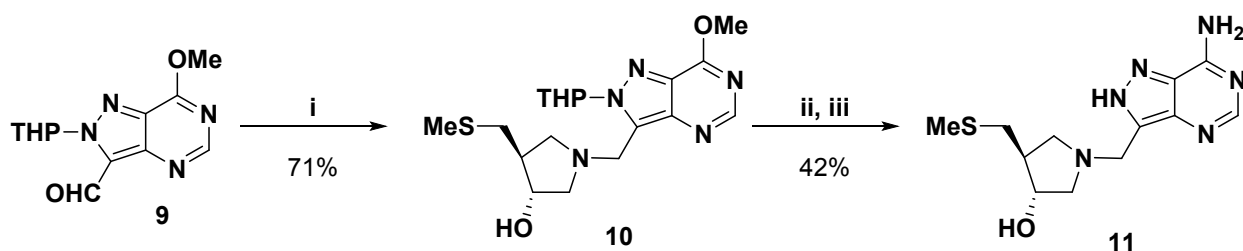
The N3 of **1** makes no catalytic site contacts in MTAP or MTAN enzymes, motivating the synthesis of a 3-deaza-analogue of **1**.^{17,23,29} Treatment of 2-hydroxy-4-methyl-3-nitropyridine (**2**) with Brederick's reagent afforded enamine **3** (Scheme 2) which with zinc in acetic acid gave 3,9-dideazahypoxanthine (**4**). This material was converted to the 6-chloro-derivative **5**, which on treatment with catalytic copper (I) chloride in aqueous ammonia afforded 3,9-dideazaadenine (**6**). Mannich reaction of **6** and pyrrolidine **7** gave the desired 3-deazaMTDIA **8**.²²



Reagents: (i) $t\text{BuOCH}(\text{NMe}_2)_2$, DMF, 100 °C; (ii) Zn, HOAc; (iii) POCl_3 , 100 °C; (iv) aq NH_3 , CuCl, 120 °C (v) HCHO, aq EtOH, 80-100 °C.

Scheme 2

During transition-state inhibitor design work for purine nucleoside phosphorylase, 8-aza-immucillins were found to be powerful inhibitors.^{26,30,31} The 8-aza-analogue of **1** was targeted for synthesis. Treatment of aldehyde **9**³² with pyrrolidine **7** and 2-methylpyridine borane complex gave **10** (Scheme 3). Ammonolysis followed by deprotection afforded 8-aza-MTDIA **11**.



Reagents: (i) Picoline borane, **7**, MeOH; (ii) 7 N NH₃/MeOH, 120 °C; (iii) aq HCl, MeOH.

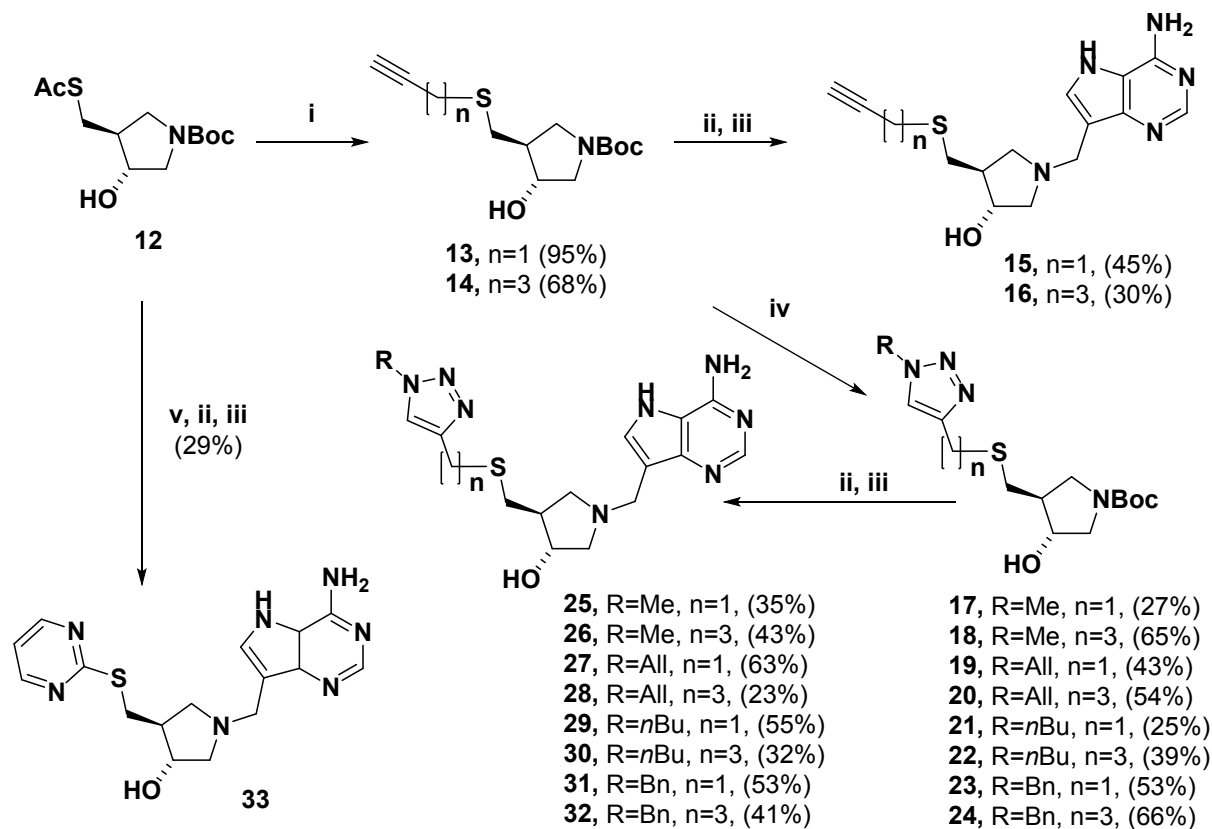
Scheme 3

Modifications in the 5'-thio substituent

Both the human MTAP and *Hp*MTAN enzymes tolerate diversity in the 5'-thio substituents – particularly for the MTANs.²⁴ With this in mind, we prepared 5'-substituted thio-MTDIA analogues by coupling 5'-alkynyl derivatives with some azides using click chemistry.

The thioacetate **12**¹⁷ was treated with sodium methoxide/methanol followed by either propargyl bromide or 5-mesyloxy-pent-1-yne to give the alkynylthio-substituted compounds **13** and **14** (Scheme 4). These compounds, after acidic treatment to remove the Boc group followed by a Mannich reaction with 9-deazaadenine, then afforded **15** and **16**. The acetylenes **13** and **14** were individually treated with methyl iodide, allyl bromide, *n*-butyl bromide or benzyl bromide along with sodium azide and catalytic copper (I) iodide affording the triazole 'click' products **17**-

24.³³ Deprotection, followed by a Mannich reaction with 9-deazaadenine³⁴ then provided the 5'-substituted thio- analogues **25-32**. The 2-pyrimidinethio analogue **33** was prepared by steps v, ii and iii (Scheme 4).



Reagents: (i) NaOMe, MeOH, 30min then 3-propargyl bromide or 5-mesyloxy-pent-1-yne; (ii) MeOH/aq HCl(conc.) 3:1 v/v; (iii) 9-deazaadenine, formaldehyde, EtOH/water, 70-100°C (microwave), 2-6h; (iv) MeI, allyl bromide, nBuBr or BnBr, NaN₃, CuI, MeOH; (v) NaOMe, MeOH, then 2-chloropyrimidine.

Scheme 4

Inhibition of MTAP and HpMTAN

Most of the compounds described here are structurally related to methylthio-DADMe-Immucillin-A (MTDIA), a transition-state inhibitor of MTAP and MTANs. Here, the varied 5'-

1
2
3 alkylthio groups yielded strong inhibitors of MTAP and *Hp*MTAN (Figure 2) with dissociation
4
5 constants (K_d values) varying by over two orders of magnitude. Tight binding of these transition-
6
7 state analogues depends on the ribocation mimic of the transition state provided by the cationic
8
9 hydroxypyrrolidine and protonation of N7 in the 9-deazaadenine, a second important feature of
10
11 the transition state structure. The 6-amino group is essential, as its loss prevents binding (Figure
12
13
14 2).

15 16 **Crystal structures of analogues with MTAP and *Hp*MTAN**

17
18 Structural analysis of inhibitors **15**, **16**, **30** and **32** bound to human MTAP and *Hp*MTAN
19
20 correlated the catalytic site interactions with the binding affinity to these enzymes (Figure 2 and
21
22 Table 1). Human MTAP and *Hp*MTAN were co-crystallized with the inhibitors and crystal
23
24 structures solved by molecular replacement using PHASER at high resolutions (Table 1).³⁵
25
26 Structure analysis using MolProbity indicated that none of the amino acid residues are outliers in
27
28 the Ramachandran plots (Table 1).³⁶
29
30
31
32

33
34 Human MTAP in complex with four inhibitors was solved at 1.62 to 1.99 Å resolutions
35
36 in different space groups using the apo human MTAP monomer as the initial phasing model in
37
38 PHASER. Human MTAP catalytic sites are located at the subunit interfaces of the trimer.
39
40 Asymmetric units of human MTAP crystals contain a monomer with **15** and **16**; and a trimer
41
42 with **30** and **32**. The trimer is the physiological state of human MTAP. Solvent accessible surface
43
44 area of the subunit-subunit interfaces is 1187 Å². The low RMSD for C α (0.357 – 0.710 Å) of
45
46 the four inhibitor-bound structures indicate only minor structural differences. MTAP monomers
47
48 contain 10 β sheets (residues are β 1, 11-16; β 2, 29-33; β 3, 45-50; β 4, 54-59; β 5, 87-98; β 6, 106-
49
50 110; β 7, 112-116; β 8, 161-164; β 9, 165-172; β 10, 210-220) with 6 α helices (from residues α 1,
51
52 73-84; α 2, 146-159; α 3, 180-189; α 4, 200-208; α 5, 233-259; α 6, 264-274; Figure S1). The
53
54
55
56
57
58
59
60

1
2
3 electron density map of the peptide backbone and amino acid side chains are clearly resolved.
4
5 Inhibitor binding is also well defined in the catalytic sites (Figure S2). The purine and
6
7 pyrrolidine rings of the four inhibitors bind in the same conformation but the 5'-alkylthio group
8
9 of **30** and **32** bind in a conformation different from **15** and **16** (Figure S3). The N1 of the
10
11 inhibitor forms a hydrogen bond with a structural water molecule while N6 forms hydrogen
12
13 bonds to the carboxyl oxygens of both Asp220 and Asp222. Asp220 also forms a hydrogen bond
14
15 interaction with N7, making it bidentate with respect to inhibitor binding. MTAP complexes of
16
17 **15** and **16** have the hydroxyl groups and N1' (corresponding to the C1' of the substrate) of the
18
19 pyrrolidine ring in hydrogen bond interactions with a phosphate oxygen and with Thr18 (Figure
20
21 3). The candidate nucleophilic oxygen (O2, nearest to the reaction center) of phosphate is
22
23 hydrogen bonded with Thr93 (OG1), Thr197 (OG1) and a water molecule. The O3 of the
24
25 phosphate is in hydrogen bond interactions with peptide nitrogens of Thr18 and Ala94.
26
27 Phosphate O4 forms hydrogen bonds with Arg60 (NH1) and His61 (NE2). These interactions are
28
29 missing in MTAP complexes with **30** and **32**, as phosphate is displaced in these structures.
30
31 Instead, a chloride ion is bound near the phosphate binding pocket and is coordinated with
32
33 Thr193 (OG1), Thr197 (OG1) and a water molecule. The 5'-alkylthio group binding mode of **15**
34
35 and **16** is different from **30** and **32**, where the extended chain folds into the phosphate binding
36
37 site (Figure 3; Table 2).
38
39
40
41
42
43
44

45 *Hp*MTAN was co-crystallized with the same inhibitors and the structures solved at
46
47 resolutions of 1.45 to 1.62 Å (Table 1). Previous and current analysis indicates a functional
48
49 dimer for *Hp*MTAN. The solvent accessible surface area of the dimer interface is 1654 Å².
50
51 *Hp*MTAN contains seven helices including one 3_{10} -helix and ten β -sheets, similar to other
52
53 MTAN structures.³⁷⁻³⁹ They are arranged in three $\alpha\beta\alpha$ -layer structures with central mixed β -
54
55
56
57
58
59
60

1
2 sheets (Figure S4). The low RMSD (0.091 – 0.195 Å) of the inhibitor complexes indicate highly
3
4 similar C α chains. Inhibitors were bound in both active sites of *Hp*MTAN with low B-factors
5
6 and clear electron density maps (Figure S5). Except for the 5'-alkylthio groups, the binding
7
8 modes of the inhibitors are similar (Figure S3). Inhibitors with extended 5'-alkylthio groups fill
9
10 the full extent of the 5'-binding pocket while short 5'-alkylthio groups do not. The binding modes
11
12 of the purine and pyrrolidine rings of the inhibitors are the same. Hydrogen bond interactions to
13
14 9-deazaadenine include the Val154 nitrogen with N1, N6 with the carbonyl oxygen of Val154
15
16 and N7 with a carboxyl oxygen of Asp198 (OD2). N7 protonation is important to transition-state
17
18 formation during the MTAN hydrolysis reaction. The structural nucleophilic water oxygen is 2.7
19
20 Å from N1', in hydrogen bond contacts with Glu13 (OE2) and Arg194 (NH1). The 3'-hydroxyl
21
22 group of the pyrrolidine is hydrogen bonded with a carboxyl oxygen of Glu175 (Figure 4).
23
24 Inhibitor 5'-alkylthio groups occupy different parts of the 5'-alkylthio binding pocket, which
25
26 extends toward the solvent exterior (Table 2 and Figure 4). Inhibitors **15** and **16** fill the 5'-
27
28 alkylthio group binding pocket to engage the most interactions with the enzyme.
29
30
31
32
33

34 35 **Structural comparisons**

36
37 Crystal structures of human MTAP with inhibitors **30** and **32** (large 5'-alkylthio groups)
38
39 differ from those with **15** and **16** (smaller 5'-alkylthio groups). Binding of **30** and **32** caused
40
41 rearrangement of the loop between β 1- β 2 (residues 17 to 28) to a more open conformation than
42
43 with **15** and **16** (Figure 5). In the complex with **15** and **16**, this loop is closed. The rearrangement
44
45 of the β 1- β 2 loop with **30** and **32** also alters the β 4- α 1 loop conformation so His61 is displaced
46
47 slightly and His65 is flipped 180°. The hydroxyl group of the pyrrolidine ring is rotated 18°
48
49 towards the outside in **30** and **32** complexes. These conformational changes alter the phosphate
50
51 binding site which is occupied by the bulky 5'-alkylthio groups. For the structural comparisons,
52
53
54
55
56
57
58
59
60

1
2 unliganded MTAP (PDB ID: 3OZE); and a complex with MTA and sulfate (PDB ID: 1CG6)
3
4 were compared.^{40,41} These structures are similar to that with inhibitors **15** and **16**.
5
6
7

8 *Hp*MTAN structures with the same four inhibitors were solved at high resolution in the
9
10 P4₁2₁2 space group (Table 1). In unliganded *E. coli* MTAN (PDB ID: 1Z5P), both catalytic sites
11
12 are in an open configuration, but in unliganded *Hp*MTAN (PDB ID: 3NM4) the binding of a Tris
13
14 buffer molecule induced a closed conformation in monomer-A with monomer-B in an open
15
16 conformation.^{39,42,43} The ligand-induced conformation change moves the β 10- α 6 loop
17
18 approximately 7 Å closer to the binding site to form the closed state. When the *Hp*MTAN bound
19
20 to **15**, **16**, **30** and **32** was compared to *p*-ClPh-Thio-DADMe-ImmA bound to *Hp*MTAN and
21
22 resolved with neutron diffraction (PDB ID: 5K1Z); hydrogen bond contacts of the DADMe-
23
24 ImmA core were found to be intact, including the N7 hydrogen sharing with Asp198.⁴⁴ All
25
26 *Hp*MTAN-inhibitor complexes are in closed configurations but differ in the 5'-alkylthio group
27
28 binding pocket (Table 2; Figs. 4, 5).
29
30
31
32
33

34 **Structure-inhibition relationship**

35
36 Inhibitors **15** and **16** gave K_d values of 0.63 and 0.94 nM, respectively, for human MTAP,
37
38 slightly better than **30** and **32**, with K_d values of 1.3 and 1.4 nM, respectively. 9-Deazaadenine of
39
40 the inhibitors is co-located in the catalytic site for the four inhibitors, while the 3'-hydroxyl group
41
42 of the pyrrolidine of **30** and **32** is shifted upward relative to **15** and **16** (Figs. S1 and S3). The 5'-
43
44 alkylthio groups of the inhibitors, important for the potency, are bound in different
45
46 conformations. Inhibitors **15** and **16** occupy the hydrophobic binding site normally occupied by
47
48 the 5'-methylthiol or 5'-homocysteinyl groups of the natural substrates. In contrast, **30** and **32**
49
50 induced β 1- β 2 loop rearrangement by exceeding the size of the 5'-alkylthio binding pocket.
51
52 Upon **30** and **32** binding, the inhibitor triazoles reposition under the 3'-hydroxypyrrolidine to
53
54
55
56
57
58
59
60

1
2
3 occupy the phosphate binding site. As **30** and **32** occupy both nucleoside and phosphate binding
4
5 sites, phosphate is not bound in the **30** and **32** MTAP complexes. Ion pair formation between the
6
7 cationic 3'-hydroxypyrrolidine ring and anionic phosphate is part of the transition-state
8
9 ensemble, contributing to tight binding of structurally compatible analogues. Remarkably, most
10
11 of the binding affinity is retained in **30** and **32** without bound phosphate.
12
13

14
15 Enzyme inhibition experiments revealed that **15**, **16**, **30** and **32** are 26 to 55 picomolar
16
17 inhibitors of *Hp*MTAN (Figure 2). The 5'-alkylthio binding site accommodates groups
18
19 approximately 10 Å extending from the 4'-carbon of the pyrrolidine group and longer groups are
20
21 accommodated as the binding channel opens to solvent. The optimal fit of **16** to the site explains
22
23 its high binding affinity, but even relatively small 5'-alkylthio groups (**15**) or bulky and
24
25 hydrophilic triazole groups (**30** and **32**) are picomolar inhibitors. In the *Hp*MTAN-**15** complex,
26
27 the unfilled space in the 5'-alkylthio binding pocket is occupied by an ethylene glycol molecule
28
29 interacting with solvent molecules and a carboxyl oxygen Asp209 (OD1). The groups of **30** and
30
31 **32** are larger, forcing them into the solvent space beyond the organized binding site. The distal
32
33 atoms of **30** and **32** are disordered, resulting in decreased affinity. Despite these differences, the
34
35 sum of the interactions provides favorable binding energy (Table 2; Figure 4).
36
37
38
39
40

41 Inhibitor catalytic site contacts in both *Hp*MTAN and MTAP show no interactions with
42
43 the N3 atom of 9-deazaadenine. In contrast, both enzymes have hydrogen bond interactions with
44
45 the protonated N7. As protonation of N7 is a feature of the transition state, this is an important
46
47 characteristic of high affinity inhibitors. A 3,9-didezaadenine inhibitor (**8**) retains the desired
48
49 protonation at N7 in a scaffold otherwise identical to MTDIA (**1**). However, (**1**) is an 86 pM
50
51 inhibitor for both *Hp*MTAN and MTAP while the dissociation constant for (**8**) increased by
52
53 >100-fold to 10 and 32 nM for *Hp*MTAN and MTAP, respectively, indicating weaker N7 to
54
55
56
57
58
59
60

1
2 enzyme interactions because of the loss of electron contribution from N3. The N6 exocyclic
3 amino group is doubly hydrogen-bonded at the catalytic sites and its replacement by O6
4 eliminates binding to the catalytic sites at concentrations of 5 μ M (**34**, **35**).
5
6
7
8
9

10 **Conclusions**

11
12 Human MTAP is a validated drug target. Its genetic deletion in 15% of all human cancers
13 makes those malignancies more susceptible to inhibitors of PRMT5, MAT2A or RIOK1.⁷⁻¹⁰
14
15 *Hp*MTAN catalyzes an essential step in menaquinone synthesis in *H. pylori* but not in common
16 gut bacteria, making it a species-specific target in the treatment of peptic ulcers. New transition-
17 state analogues of *Hp*MTAN and MTAP were synthesized to explore variations of the MT-
18 DADMe-Immucillin-A chemical scaffold and the structure-function relationship to these target
19 enzymes. The 4'-position of the 3'-hydroxypyrrolidine ring of DADMe-Immucillin-A was varied
20 by click-chemistry addition of varied substituents. Inhibition constants indicated the best
21 compounds (**15** and **16**) to be picomolar inhibitors against both MTAP and *Hp*MTAN, with 12 to
22 36-fold preference for the *Hp*MTAN. Bulky 4'-substituents (eg. **25** – **29** and **33**) showed a 92- to
23 243-fold preference for *Hp*MTAN. The hydrophobic pocket accepting the 4'-substituent in
24 *Hp*MTAN can accommodate methylthio (in MTA), homocysteine (in SAH) and the bulky side
25 chain of aminofutalosine. It does so in a hydrophobic tunnel that opens towards solvent. Human
26 MTAP has a more restricted 4'-binding pocket that accepts only the methylthio and
27 homocysteine groups. Larger substituents fold under the 3'-hydroxypyrrolidine ring and occupy
28 the phosphate binding site, while retaining other contacts to the 9-deazaadenine and
29 hydroxypyrrolidine that dominate the transition state binding energy. Four transition-state
30 analogues were co-crystallized with MTAP and *Hp*MTAN. Structural analysis revealed that
31 binding of **30** and **32** to human MTAP caused the structural rearrangement to displace phosphate
32
33
34
35
36
37
38
39
40
41
42
43
44
45
46
47
48
49
50
51
52
53
54
55
56
57
58
59
60

1
2 and accommodate long and bulky 5'-alkylthio groups. With *Hp*MTAN, inhibitor **16** takes full
3 advantage of the *Hp*MTAN binding pocket, and thus binds more tightly than other inhibitors.
4
5

6 7 8 **MATERIALS AND METHODS**

9 10 11 **Chemical synthesis of transition-state analogues**

12
13
14 The MTDIA chemical scaffold was explored by synthesizing a new generation of
15 transition-state analogues for *Hp*MTAN and MTAP. The 4'-position of the 3'-hydroxypyrrolidine
16 ring of MTDIA was varied by click-chemistry. All reactions were performed under an argon or
17 nitrogen atmosphere, unless water was used as solvent or the reaction mixture was heated above
18 100 °C. All final compounds gave satisfactory purity ($\geq 95\%$) by HPLC and by ^1H and ^{13}C NMR.
19 Details of the chemical synthesis are provided in the supplementary information.
20
21
22
23
24
25
26
27
28

29 **Expression and purification of human MTAP**

30
31 Human MTAP was prepared as previously described with some modifications.⁴¹ In brief,
32 a plasmid containing the coding region for MTAP was transformed into BL21-CodonPlus(DE3)-
33 RIPL *E. coli* chemically competent cells. Nucleotide sequencing validated the DNA sequence for
34 MTAP. The culture was grown at 37 °C and 200 rpm in LB medium containing 100 $\mu\text{g}/\text{mL}$
35 ampicillin. Heterologous protein expression was induced when OD_{600} reached 0.6-0.8 by
36 addition of 1 mM IPTG (final concentration). After 8 h induction at 37 °C and 200 rpm, the cells
37 were harvested by centrifugation (5,000 $\times g$ for 20 min) and stored at -80 °C. All subsequent
38 steps were carried out at 4 °C, unless stated otherwise.
39
40
41
42
43
44
45
46
47
48
49

50
51 The pellet was suspended in lysis buffer (50 mM HEPES-NaOH, 5 mM imidazole at pH
52 7.0) (2.5 mL/g of cell pellet) with addition of protease inhibitor cComplete Mini EDTA-free (one
53 tablet per 20 g of cell pellet; Roche) and homogenized by stirring for 30 min. A spatula tip of
54
55
56
57
58
59
60

1
2 lysozyme (Sigma) and DNase I (Sigma) was added to the mixture and, after 30 min stirring,
3
4 cells were disrupted by sonication (15 sec on, 15 sec off, at 30% amplitude for 30 min) and
5
6 centrifuged (20,000 x g for 20 min) to remove cell debris. The recombinant MTAP contains 14
7
8 additional amino acids at N-terminus of the native enzyme, including a His₆ tag (and a TEV
9
10 protease cleavage site). The supernatant was incubated with Ni-NTA agarose (1.0 mL of slurry/g
11
12 of cell pellet; Qiagen) for 45 min with rocking, and the mixture was poured into an empty
13
14 column and washed with 12 column volumes of cell lysis buffer. The collection of 4 column
15
16 volume fractions from a 50 to 500 mM imidazole stepwise elution gradient gave proteins
17
18 analyzed by sodium dodecyl sulfate-polyacrylamide gel electrophoresis (SDS-PAGE) (200 V
19
20 and 185 mA for 60 min in MOPS running buffer) analysis, and the fractions containing the target
21
22 protein with purity over 95% (150 to 500 mM imidazole) were pooled. Purified MTAP contains
23
24 adenine which was removed by dialysis against 50 mM HEPES-NaOH at pH 7.0 with 0.2%
25
26 (m/v) activated charcoal (Sigma) overnight using 10 kDa dialysis cassettes (Thermo Scientific).
27
28 Adenine analysis in MTAP involved denaturation with 10% (v/v) perchloric acid. Denatured
29
30 protein was removed by centrifugation and the concentration of adenine in the supernatant was
31
32 tested by spectrophotometry. Adenine-free MTAP was concentrated to approximately 300 μM or
33
34 10 mg mL⁻¹ (extinction coefficient is estimated to be 30.94 mM⁻¹ cm⁻¹ at 280 nm), and aliquots
35
36 were frozen in liquid nitrogen and stored at -80 °C. A total of 21 mg of protein was obtained
37
38 from 10 L of culture.

39 40 41 42 43 44 45 46 47 **Expression and purification of *Hp*MTAN**

48
49 *Hp*MTAN was prepared as previously described with some modifications.^{16,17} Briefly,
50
51 the plasmid containing His-tag *Hp*MTAN gene was transformed into BL21 (DE3) *E. coli*
52
53 chemically competent cells. Nucleotide sequencing validated the DNA sequence for *Hp*MTAN.
54
55
56
57
58
59
60

1
2
3 The culture was grown at 37 °C and 200 rpm in LB medium containing 50 µg/mL ampicillin,
4 and heterologous protein expression was induced when OD₆₀₀ reached 0.6-0.8 by addition of 0.5
5 mM IPTG (final concentration). Temperature was lowered to 30 °C upon addition of IPTG, and
6
7 the culture was grown an additional 20 h. Cells were harvested by centrifugation (5,000 x g for
8
9 20 min) and stored at -80 °C. All subsequent steps were carried out at 4 °C, unless stated
10
11 otherwise. The purification of *Hp*MTAN was the same as described above for MTAP. A total of
12
13 210 mg of protein was obtained from 2 L of culture.
14
15
16
17
18

19 **Inhibition assays of MTAP**

20
21
22 MTAP catalytic activity was measured using the absorbance difference between MTA
23 and adenine.⁴¹ A second assay followed the conversion of MTA to 2,8-dihydroxyadenine based
24 on the oxidation of adenine by xanthine oxidase to give an absorbance change at 305 nm ($\epsilon_{305} =$
25 $15.5 \text{ mM}^{-1}\text{cm}^{-1}$). Inhibition constants were analyzed by fitting rate data to the Morrison quadratic
26 equation.⁴⁵ Reactions in a 1 mL cuvette containing 100 mM K₂PO₄, 1 mM DTT, 800 µM MTA,
27 3 nM MTAP, 1 unit of xanthine oxidase, and varying concentrations of each inhibitor.
28
29 Equilibrium dissociation constants were determined from reaction rates inhibition following
30 slow-onset binding (K_i^*). The rates of each reaction were taken 40 min after initiation of the
31 reaction, a time when slow-onset equilibrium had occurred.
32
33
34
35
36
37
38
39
40
41
42

43 **Inhibition assays of *Hp*MTAN**

44
45 Inhibition constants were determined as above. Reactions (1 mL) contained 100 mM
46 HEPES pH 7.2, 1 mM DTT, 100 mM NaCl, 1 mM MTA, 0.6 nM *Hp*MTAN, 1 unit of xanthine
47 oxidase, and varying concentrations of each inhibitor (0 to 100 µM). Reactions were monitored
48 as described above for MTAP to obtain the inhibition constants following slow-onset binding
49
50
51
52
53
54
55
56
57
58
59
60

1
2 when appropriate (K_i^*). The rates of each reaction were taken 40 minutes after initiation of the
3
4 reaction, to a time when slow-onset equilibrium had occurred.
5
6

7 **Co-crystallization with transition-state inhibitors**

8

9 Co-crystallization of MTAP and *Hp*MTAN with four tight binding transition-state
10 inhibitors (**15**, **16**, **30**, and **32**) used sitting drop vapor diffusion at 22 °C. MTAP or *Hp*MTAN (5
11 mg/ml) was mixed with inhibitors in a 1:2 molar ratio and incubated for two hours on ice. The
12
13 proteins were screened for crystal-forming conditions with the Microlytic (MCSG1-4) and
14 Hampton (crystal screenHT) kits. Crystallization trials were in 96-well INTELLI plates using the
15
16 CRYSTAL-GRYPHON crystallization robot (ART ROBBINS). Crystallization drops contained
17
18 0.5 μ L of enzyme-inhibitor mixture and 0.5 μ L of well solution. The volume of the well solution
19
20 was 70 μ L. Good quality crystals were obtained in one week (Table 1).
21
22
23
24
25
26
27

28 **Data Collection and Processing**

29

30 Diffraction data were collected at the LRL-CAT beam line (Argonne National
31 Laboratory, Argonne, IL) at a wavelength of 0.97931 Å (Table 1). Data were processed using the
32
33 iMOSFLM program and scaled by the AIMLESS program in the CCP4 suite, using the
34
35 appropriate space group (Table 1).^{46,47} Data quality was analyzed using the SFCHECK and
36
37 XTRIAGE.^{47,48} Matthews coefficient (V_m) calculations indicated the number of monomers
38
39 present in the unit cells.
40
41
42
43

44 **Structure Determination and Refinement**

45

46 Crystal structures of MTAP and *Hp*MTAN in complex with transition-state analogue
47
48 inhibitors were solved by molecular replacement using PHASER.³⁵ Chain-A of wild-type MTAP
49
50 (PDB ID: 5TC6) and *Hp*MTAN (PDB ID: 4WKP) structures were used as the initial phasing
51
52 model. The model obtained from PHASER was manually adjusted and completed using the
53
54 graphics program COOT.⁴⁹ Structure refinement was performed with REFMAC5, using standard
55
56
57
58
59
60

1
2 protocols for the NCS refinement.⁵⁰ Inhibitor molecules were deleted from the models to initiate
3 the refinement. After water was added, inhibitor molecules were fitted into their electron
4 densities (Table 1).
5
6
7
8

9 **Structure Analysis**

10
11 Crystal structures of unliganded wild-type MTAP (PDB ID: 3OZE, chain: B), *Hp*MTAN
12 (PDB ID: 3NM4, chain: B) and *Ec*MTAN (PDB ID: 1Z5P, chain: A) were used for structure
13 comparisons. The MTA complex with MTAP (PDB ID: 3T94) and p-ClPh-Thio-DADMe-ImmA
14 complex with *Hp*MTAN (PDB ID: 5K1Z) were also used in the structural comparisons. All
15 structural superimpositions used the SSM protocol of COOT and the geometry analyses of the
16 final model used MolProbity.³⁶ Additional structure analyses, including the calculation of the B-
17 factor profiles used BAVEGAGE of the CCP4 suite.⁴⁷ Structural figures were generated with the
18 molecular graphics program PyMOL. For MTAP and *Hp*MTAN structures, subunit-A was used
19 for all the structural analyses and comparisons.
20
21
22
23
24
25
26
27
28
29
30
31
32
33
34

35 **ACKNOWLEDGMENTS**

36
37
38 This project was supported by research grant GM041916 from the National Institutes of
39 Health and the New Zealand Foundation for Research Science and Technology contract
40 C08X0701. The Albert Einstein Crystallographic Core X-Ray diffraction facility is supported by
41 NIH Shared Instrumentation Grant S10 OD020068. Data collection also involved resources of
42 the Advanced Photon Source, a U.S. Department of Energy (DOE) Office of Science User Facility
43 operated for the DOE Office of Science by Argonne National Laboratory under Contract No. DE-
44 AC02-06CH11357. Use of the Lilly Research Laboratories Collaborative Access Team (LRL-
45
46
47
48
49
50
51
52
53
54
55
56
57
58
59
60

CAT) beamline at Sector 31 of the Advanced Photon Source was provided by Eli Lilly Company, which operates the facility.

AUTHOR INFORMATION

Corresponding Author

* E-mail: vern.schramm@einstein.yu.edu or peter.tyler@vuw.ac.nz

ORCID

Rajesh K. Harijan: 0000-0003-1503-5057

Rodrigo G. Ducati: 0000-0002-8783-8847

Peter C. Tyler: 0000-0002-3151-6208

Gary B. Evans: 0000-0002-6973-2002

Vern L. Schramm: 0000-0002-8056-1929

Oskar Hoff: 0000-0002-7716-7242

NOTES

The authors declare no competing financial interest.

AUTHOR CONTRIBUTIONS

V.L.S. and P.C.T. supervised the project. O.H. synthesized the transition-state analogues.

R.G.D., R.S.F. and B.M.H expressed, purified the enzymes and determined the enzyme kinetics.

R.K.H. conducted the structure determinations and characterizations. R.K.H., R.G.D, P.C.T and

V.L.S. wrote the paper. All the authors were involved in reviewing the data and manuscript drafts.

STRUCTURAL DATA

1
2 PDB ID CODES: 6DYZ, 6DZ0, 6DZ3, 6DZ2, 6DYU, 6DYV, 6DYY, 6DYW. Authors will
3
4 release the atomic coordinates and experimental data upon article publication.
5
6

7 **SUPPORTING INFORMATION CONTENT**

8
9 Page S1: Title page and abbreviations
10

11 Page S2: Index to Supplementary Information Content
12

13
14 Page S3: Figure S1. Human MTAP subunit ribbon structure comparing free and liganded
15
16 enzyme.
17

18 Page S4: Figure S2. Electron density omit maps for MTAP-inhibitor complexes of **15, 16, 30,**
19
20 **32.**
21

22
23 Page S5: Figure S3. Inhibitor geometry at the catalytic sites of human MTAP and *Hp*MTAN.
24

25 Page S6: Figure S4. *Hp*MTAN subunit ribbon structures comparing free and liganded MTANs.
26

27
28 Page S7: Figure S5. Electron density omit maps for *Hp*MTAN-inhibitor complexes of **15, 16,**
29
30 **30, 32.**
31

32 Page S8: Table S1. Crystallization and crystal handling
33

34 Pages S9 – 33: Details of chemical synthesis
35

36
37 Page S34: SMILES formula data for all inhibitions indexed by compound number
38

39 Pages S35 – 47: NMR spectra of all inhibitors
40
41
42
43
44
45
46
47
48
49
50
51
52
53
54
55
56
57
58
59
60

1
2
3 **ABBREVIATIONS:** MTDIA: methylthio-DADMe-Immucillin-A; MTA: *S*-methyl-5'
4 thioadenosine; All: allyl; DQF-COSY: double-quantum filtered correlation spectroscopy; Q-
5 TOF: quadrupole time-of-flight; MTAN: 5'-methylthioadenosine/*S*-adenosylhomocysteine
6 nucleosidase; *Hp*MTAN: *Helicobacter pylori* MTAN; MTAP: 5'-methylthioadenosine
7 phosphorylase; MTR: 5-methylthio- α -D-ribose 1-phosphate; SAM: *S*-Adenosylmethionine;
8 SAH: *S*-adenosylhomocysteine, SRH: *S*-ribosylhomocysteine; NMR: nuclear magnetic
9 resonance; HPLC: high performance liquid chromatography; RT: room temperature; t-Bu: tert-
10 butyl; DMF: dimethylformamide; aq: aqueous; Et: ethyl; Me: methyl; THP: tetrahydropyranyl;
11 BOC: tert-butyloxycarbonyl; Ac: acyl; n-Bu: n-butyl; Bn: benzyl; PRMT5: protein arginine
12 methyltransferase 5; MAT2A: *S*-adenosylmethionine synthetase 2A; HSQC: heteronuclear single
13 quantum coherence spectroscopy; DEPT: distortionless enhancement by polarization transfer;
14 APT: Attached proton test
15
16
17
18
19
20
21
22
23
24
25
26
27
28
29
30
31
32
33
34
35
36
37
38
39
40
41
42
43
44
45
46
47
48
49
50
51
52
53
54
55
56
57
58
59
60

1
2
3
4
5
6
7
8
9
10
11
12
13
14
15
16
17
18
19
20
21
22
23
24
25
26
27
28
29
30
31
32
33
34
35
36
37
38
39
40
41
42
43
44
45
46
47
48
49
50
51
52
53
54
55
56
57
58
59
60
REFERENCES

1. Lieber, C. S.; Packer, L. S-Adenosylmethionine: Molecular, Biological, and Clinical Aspects--an Introduction. *Am. J. Clin. Nutr.* **2002**, *76*, 1148S-1150S.
2. Loenen, W. A. M. S-Adenosylmethionine: Jack of All Trades and Master of Everything? *Biochem. Soc. Trans.* **2006**, *34*, 330–333.
3. Battaglia, V.; DeStefano Shields, C.; Murray-Stewart, T.; Casero, R. A., Jr. Polyamine Catabolism in Carcinogenesis: Potential Targets for Chemotherapy and Chemoprevention. *Amino Acids* **2014**, *46*, 511–519.
4. Tabor, C. W.; Tabor, H. Polyamines. *Annu.Rev.Biochem.* **1984**, *53*, 749–790.
5. Basu, I.; Cordovano, G.; Das, I.; Belbin, T. J.; Guha, C.; Schramm, V. L. A Transition State Analogue of 5'-Methylthioadenosine Phosphorylase Induces Apoptosis in Head and Neck Cancers. *J.Biol.Chem.* **2007**, *282*, 21477–21486.
6. Basu, I.; Locker, J.; Cassera, M. B.; Belbin, T. J.; Merino, E. F.; Dong, X.; Hemeon, I.; Evans, G. B.; Guha, C.; Schramm, V. L. Growth and Metastases of Human Lung Cancer Are Inhibited in Mouse Xenografts by a Transition State Analogue of 5'-Methylthioadenosine Phosphorylase. *J.Biol.Chem.* **2011**, *286*, 4902–4911.
7. Mavrakis, K. J.; McDonald, E. R. 3rd.; Schlabach, M. R.; Billy, E.; Hoffman, G. R.; deWeck, A.; Ruddy, D. A.; Venkatesan, K.; Yu J.; McAllister, G.; Stump, M.; deBeaumont, R.; Ho, S.; Yue, Y.; Liu, Y.; Yan-Neale, Y.; Yang, G.; Lin, F.; Yin, H.; Gao, H.; Kipp, D. R.; Zhao, S.; McNamara, J. T.; Sprague, E. R.; Zheng, B.; Lin, Y.; Cho, Y. S.; Gu, J.; Crawford, K.; Ciccone, D.; Vitari, A. C.; Lai, A.; Capka, V.; Hurov, K.; Porter, J. A.; Tallarico, J.; Mickanin, C.; Lees, E.; Pagliarini, R.; Keen, N.; Schmelzle, T.; Hofmann, F.; Stegmeier, F.; Sellers, W. R. Disordered Methionine Metabolism in

- 1
2
3 MTAP/CDKN2A-Deleted Cancers Leads to Dependence on PRMT5. *Science* **2016**, *351*,
4
5 1208-1213.
6
7
- 8 8. Kryukov, G. V.; Wilson, F. H.; Ruth, J. R.; Paulk, J.; Tsherniak, A.; Marlow, S. E.;
9
10 Vazquez, F.; Weir, B. A.; Fitzgerald, M. E.; Tanaka, M.; Bielski, C. M.; Scott, J. M.;
11
12 Dennis, C.; Cowley, G. S.; Boehm, J. S.; Root, D. E.; Golub, T. R.; Clish, C. B.; Bradner,
13
14 J. E.; Hahn, W. C.; Garraway, L. A. MTAP Deletion Confers Enhanced Dependency on
15
16 the PRMT5 Arginine Methyltransferase in Cancer Cells. *Science* **2016**, *351*, 1214-1218.
17
18
- 19 9. Pfister, S. X.; Ashworth, A. Marked for Death: Targeting Epigenetic Changes in Cancer.
20
21
22 *Nat. Rev. Drug Disc.* **2017**, *16*, 241-263.
23
- 24 10. Marjon, K.; Cameron, M.J.; Quang, P.; Clasquin, M.F.; Mandley, E.; Kunii, K.; McVay,
25
26 M.; Choe, S.; Kernysky, A.; Gross, S.; Konteatis, Z.; Murtie, J.; Blake, M. L.; Travins, J.;
27
28 Dorsch, M.; Biller, S. A.; Marks, K. M. MTAP Deletions in Cancer Create Vulnerability
29
30 to Targeting of the MAT2A/PRMT5/RIOK1 Axis. *Cell Rep.* **2016**, *15*, 574-587.
31
32
33
- 34 11. Parveen, N.; Cornell, K. A. Methylthioadenosine/S-Adenosylhomocysteine Nucleosidase,
35
36 a Critical Enzyme for Bacterial Metabolism. *Mol.Microbiol.* **2011**, *79*, 7–20.
37
38
- 39 12. Chen, X.; Schauder, S.; Potier, N.; Van Dorsselaer, A.; Pelczer, I.; Bassler, B. L.;
40
41 Hughson, F. M. Structural Identification of a Bacterial Quorum-Sensing Signal Containing
42
43 Boron. *Nature* **2002**, *415*, 545–549.
44
- 45 13. Xavier, K. B.; Bassler, B. L. LuxS Quorum Sensing: More than Just a Numbers Game.
46
47
48 *Curr.Opin.Microbiol.* **2003**, *6*, 191–197.
49
- 50 16. Wang, S.; Haapalainen, A. M.; Yan, F.; Du, Q.; Tyler, P. C.; Evans, G. B.; Rinaldo-
51
52 Matthis, A.; Brown, R. L.; Norris, G. E.; Almo, S. C.; Schramm, V. L. A Picomolar
53
54
55
56
57
58
59
60

- 1
2
3 Transition State Analogue Inhibitor of MTAN as a Specific Antibiotic for *Helicobacter*
4
5 *pylori*. *Biochemistry* **2012**, *51*, 6892–6894.
6
7 17. Wang, S.; Cameron, S. A.; Clinch, K.; Evans, G. B.; Wu, Z.; Schramm, V. L.; Tyler, P. C.
8
9 New Antibiotic Candidates against *Helicobacter pylori*. *J.Am.Chem.Soc.* **2015**, *137*,
10
11 14275–14280.
12
13 18. Schramm, V. L. Enzymatic Transition States, Transition-State Analogs, Dynamics,
14
15 Thermodynamics, and Lifetimes. *Annu.Rev.Biochem.* **2011**, *80*, 703–732.
16
17 19. Singh, V.; Schramm, V. L. Transition-State Structure of Human 5'-Methylthioadenosine
18
19 Phosphorylase. *J.Am.Chem.Soc.* **2006**, *128*, 14691–14696.
20
21
22 20. Gutierrez, J. A.; Luo, M.; Singh, V.; Li, L.; Brown, R. L.; Norris, G. E.; Evans, G. B.;
23
24 Furneaux, R. H.; Tyler, P. C.; Painter, G. F.; Lenz, D. H.; Schramm, V. L. Picomolar
25
26 Inhibitors as Transition-State Probes of 5'-Methylthioadenosine Nucleosidases. *ACS*
27
28 *Chem.Biol.* **2007**, *2*, 725–734.
29
30
31 21. Singh, V.; Lee, J. E.; Nunez, S.; Howell, P. L.; Schramm, V. L. Transition State Structure
32
33 of 5'-Methylthioadenosine/S-Adenosylhomocysteine Nucleosidase from *Escherichia coli*
34
35 and Its Similarity to Transition State Analogues. *Biochemistry* **2005**, *44*, 11647–11659.
36
37
38 22. Evans, G. B.; Furneaux, R. H.; Lenz, D. H.; Painter, G. F.; Schramm, V. L.; Singh, V.;
39
40 Tyler, P. C. Second Generation Transition State Analogue Inhibitors of Human 5'-
41
42 Methylthioadenosine Phosphorylase. *J.Med.Chem.* **2005**, *48*, 4679–4689.
43
44
45 23. Haapalainen, A. M.; Thomas, K.; Tyler, P. C.; Evans, G. B.; Almo, S. C.; Schramm, V. L.
46
47 *Salmonella enterica* MTAN at 1.36 Å Resolution: A Structure-Based Design of
48
49 Grouped Transition State Analogs. *Structure* **2013**, *21*, 963–974.
50
51
52
53
54
55
56
57
58
59
60

- 1
2
3 24. Longshaw, A. I.; Adanitsch, F.; Gutierrez, J. A.; Evans, G. B.; Tyler, P. C.; Schramm, V.
4
5 L. Design and Synthesis of Potent “Sulfur-Free” Transition State Analogue Inhibitors of
6
7 5'-Methylthioadenosine Nucleosidase and 5'-Methylthioadenosine Phosphorylase.
8
9 *J.Med.Chem.* **2010**, *53*, 6730–6746.
10
11
12 25. Singh, V.; Evans, G. B.; Lenz, D. H.; Mason, J. M.; Clinch, K.; Mee, S.; Painter, G. F.;
13
14 Tyler, P. C.; Furneaux, R. H.; Lee, J. E.; Howell, P. L.; Schramm, V. L. Femtomolar
15
16 Transition State Analogue Inhibitors of 5'-Methylthioadenosine/S-Adenosylhomocysteine
17
18 Nucleosidase from *Escherichia coli*. *J. Biol. Chem.* **2005**, *280*, 18265–18273.
19
20
21
22 26. Evans, G. B.; Furneaux, R. H.; Schramm, V. L.; Singh, V.; Tyler, P. C. Targeting the
23
24 Polyamine Pathway with Transition-State Analogue Inhibitors of 5'-Methylthioadenosine
25
26 Phosphorylase. *J.Med.Chem.* **2004**, *47*, 3275–3281.
27
28
29 27. Singh, V.; Schramm, V. L. Transition-State Analysis of *S. pneumoniae* 5'-
30
31 Methylthioadenosine Nucleosidase. *J. Am. Chem. Soc.* **2007**, *129*, 2783-2795.
32
33
34 28. Namanja-Magliano, H. A.; Stratton, C. F.; Schramm, V. L. Transition State Structure and
35
36 Inhibition of Rv0091, a 5'-Deoxyadenosine/5'-methylthioadenosine Nucleosidase from
37
38 *Mycobacterium tuberculosis*. *ACS Chem. Biol.* **2016**, *11*, 1669-1676.
39
40
41 29. Singh, V.; Shi, W.; Evans, G. B.; Tyler, P. C.; Furneaux, R. H.; Almo, S. C.; Schramm,
42
43 V. L. Picomolar Transition State Analogue Inhibitors of Human 5'-Methylthioadenosine
44
45 Phosphorylase and X-Ray Structure with MT-Immucillin-A. *Biochemistry* **2004**, *43*, 9-
46
47 18.
48
49
50 30. Evans, G. B.; Furneaux, R. H.; Schramm, V. L.; Singh, V.; Tyler, P. C. Targeting the
51
52 Polyamine Pathway with Transition-State Analogue Inhibitors of 5'-Methylthioadenosine
53
54 Phosphorylase. *J. Med. Chem.* **2004**, *47*, 3275-3281.
55
56
57
58
59
60

- 1
2
3 31. Kicska, G. A.; Tyler, P. C.; Evans, G. B.; Furneaux, R. H.; Shi, W.; Fedorov, A.;
4
5 Lewandowicz, A.; Cahill, S. M.; Almo, S. C.; Schramm, V. L. Atomic Dissection of the
6
7 Hydrogen Bond Network for Transition-State Analogue Binding to Purine Nucleoside
8
9 Phosphorylase. *Biochemistry* **2002**, *41*, 14489-14498.
10
11
12 32. Evans, G. B.; Furneaux, R. H.; Lewandowicz, A.; Schramm, V. L.; Tyler, P. C.,
13
14 Synthesis of Second-Generation Transition State Analogues of Human Purine Nucleoside
15
16 Phosphorylase, *J. Med. Chem.*, **2003**, *46*, 5271-5276.
17
18
19 33. Rostovtsev, V. V.; Green, L. G.; Fokin, V. V.; Sharpless, K. B., A Stepwise Huisgen
20
21 Cycloaddition Process: Copper (I)-Catalyzed Regioselective “Ligation” of Azides and
22
23 Terminal Alkynes, *Angew. Chem.*, **2002**, *114*, 2708-2711.
24
25
26 34. Evans, G. B.; Cameron, S. A.; Luxenburger, A.; Guan, R.; Suarez, J.; Thomas, K.;
27
28 Schramm, V. L.; Tyler, P. C., Tight Binding Enantiomers of Pre-Clinical Drug
29
30 Candidates, *Bioorg Med Chem*, **2015**, *23*, 5326-5333.
31
32
33 35. McCoy, A. J.; Grosse-Kunstleve, R. W.; Adams, P. D.; Winn, M. D.; Storoni, L. C.; Read,
34
35 R. J. Phaser Crystallographic Software. *J. Appl. Crystallogr.* **2007**, *40*, 658–674.
36
37
38 36. Chen, V. B.; Arendall, W. B., 3rd; Headd, J. J.; Keedy, D. A.; Immormino, R. M.; Kapral,
39
40 G. J.; Murray, L. W.; Richardson, J. S.; Richardson, D. C. MolProbity: All-Atom Structure
41
42 Validation for Macromolecular Crystallography. *Acta Crystallogr. D Biol. Crystallogr.*
43
44 **2010**, *66*, 12–21.
45
46
47 37. Kim, R. Q.; Offen, W. A.; Davies, G. J.; Stubbs, K. A. Structural Enzymology of
48
49 *Helicobacter pylori* Methylthioadenosine Nucleosidase in the Futasine Pathway. *Acta*
50
51 *Crystallogr. D Biol. Crystallogr.* **2014**, *70*, 177–185.
52
53
54
55
56
57
58
59
60

- 1
2
3 38. Mishra, V.; Ronning, D. R. Crystal Structures of the *Helicobacter pylori* MTAN Enzyme
4 Reveal Specific Interactions between S-Adenosylhomocysteine and the 5'-Alkylthio
5 Binding Subsite. *Biochemistry* **2012**, *51*, 9763–9772.
6
7
8
9 39. Ronning, D. R.; Iacopelli, N. M.; Mishra, V. Enzyme-Ligand Interactions That Drive
10 Active Site Rearrangements in the *Helicobacter pylori* 5'-Methylthioadenosine/S-
11 Adenosylhomocysteine Nucleosidase. *Protein Sci.* **2010**, *19*, 2498–2510.
12
13
14
15
16 40. Appleby, T. C.; Erion, M. D.; Ealick, S. E. The Structure of Human 5'-Deoxy-5'-
17 Methylthioadenosine Phosphorylase at 1.7 Å Resolution Provides Insights into Substrate
18 Binding and Catalysis. *Structure* **1999**, *7*, 629–641.
19
20
21
22
23 41. Guan, R.; Ho, M.-C.; Brenowitz, M.; Tyler, P. C.; Evans, G. B.; Almo, S. C.; Schramm,
24 V. L. Entropy-Driven Binding of Picomolar Transition State Analogue Inhibitors to
25 Human 5'-Methylthioadenosine Phosphorylase. *Biochemistry* **2011**, *50*, 10408–10417.
26
27
28
29
30 42. Lee, J. E.; Cornell, K. A.; Riscoe, M. K.; Howell, P. L. Structure of *E. coli* 5'-
31 Methylthioadenosine/S-Adenosylhomocysteine Nucleosidase Reveals Similarity to the
32 Purine Nucleoside Phosphorylases. *Structure* **2001**, *9*, 941–953.
33
34
35
36
37 43. Lee, J. E.; Smith, G. D.; Horvatin, C.; Huang, D. J. T.; Cornell, K. A.; Riscoe, M. K.;
38 Howell, P. L. Structural Snapshots of MTA/AdoHcy Nucleosidase Along the Reaction
39 Coordinate Provide Insights into Enzyme and Nucleoside Flexibility During Catalysis.
40
41
42
43
44 *Journal of Molecular Biology* **2005**, *352*, 559–574.
45
46 44. Banco, M. T.; Mishra, V.; Ostermann, A.; Schrader, T. E.; **Evans, G. B.**; Kovalevsky, A.;
47 Ronning, D. R. Neutron Structures of the *Helicobacter pylori* 5'-Methylthioadenosine
48 Nucleosidase Highlight Proton Sharing and Protonation States. *Proc Natl Acad Sci U S A.*
49
50
51
52
53 **2016** *113*, 13756-13761.
54
55
56
57
58
59
60

- 1
2
3 45. Morrison, J. F.; Walsh, C. T. The Behavior and Significance of Slow-Binding Enzyme
4
5 Inhibitors. *Adv. Enzymol. Relat. Areas Mol. Biol.* **1988**, *61*, 201-301.
6
7 46. Battye, T. G.; Kontogiannis, L.; Johnson, O.; Powell, H. R.; Leslie, A. G. IMOSFLM: A
8
9 New Graphical Interface for Diffraction-Image Processing with MOSFLM. *Acta*
10
11 *Crystallogr.D Biol.Crystallogr.* **2011**, *67*, 271–281.
12
13 47. Collaborative Computational Project, N. 4. The CCP4 Suite: Programs for Protein
14
15 Crystallography. *Acta Crystallogr.D Biol.Crystallogr.* **1994**, *50*, 760–763.
16
17 48. Adams, P. D.; Afonine, P. V.; Bunkoczi, G.; Chen, V. B.; Davis, I. W.; Echols, N.; Headd,
18
19 J. J.; Hung, L. W.; Kapral, G. J.; Grosse-Kunstleve, R. W.; McCoy, A. J.; Moriarty, N.
20
21 W.; Oeffner, R.; Read, R. J.; Richardson, D. C.; Richardson, J. S.; Terwilliger, T. C.;
22
23 Zwart, P. H. PHENIX: A Comprehensive Python-Based System for Macromolecular
24
25 Structure Solution. *Acta Crystallogr.D Biol.Crystallogr.* **2010**, *66*, 213–221.
26
27 49. Emsley, P.; Lohkamp, B.; Scott, W. G.; Cowtan, K. Features and Development of Coot.
28
29 *Acta Crystallogr.D Biol.Crystallogr.* **2010**, *66*, 486–501.
30
31 50. Murshudov, G. N.; Vagin, A. A.; Dodson, E. J. Refinement of Macromolecular Structures
32
33 by the Maximum-Likelihood Method. *Acta Crystallogr.D Biol.Crystallogr.* **1997**, *53*,
34
35 240–255.
36
37
38
39
40
41
42
43
44
45
46
47
48
49

50 FIGURE LEGENDS

51
52
53 **Figure 1.** The transition states and reactions catalyzed by MTAP and *Hp*MTAN. (A) MTAP catalyzes the reaction
54
55 via a ribocationic transition state and phosphate as the nucleophile. Adenine and methylthio- α -D-ribose 1-phosphate
56
57
58
59
60

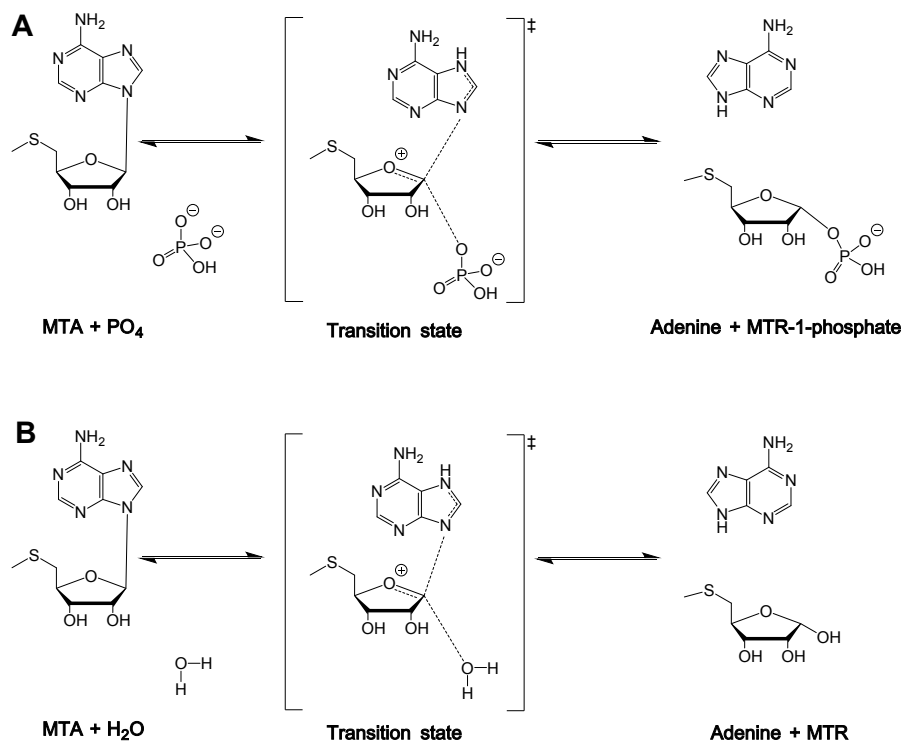
1
2 are the products. Bonds to the leaving group and the attacking nucleophile are weak, less than 0.1 Pauling bond
3 order, making the reaction more S_N1 than S_N2 in character. (B) *Hp*MTAN also catalyzes its reaction via a
4 ribocationic transition state. Water acts as the nucleophile. Adenine and methylthio-D-ribose are the products.
5
6

7
8
9 **Figure 2.** Transition-state analogue inhibitors of MTAP and *Hp*MTAN. Inhibitors were ranked based on their K_d
10 value for MTAP. ND means inhibition not detected at 5 μ M inhibitor concentration. The specificity ratio (K_d Hs/*Hp*)
11 is the affinity for human MTAP relative to *Hp*MTAN.
12
13

14
15 **Figure 3.** Stereoview of the binding sites of MTAP in complex with transition-state analogue inhibitors. The
16 inhibitor complexes of **15**, **16**, **30** and **32** are shown in panels A, B, C and D, respectively. The residues interacting
17 with inhibitors from monomer-A are shown in green and from the neighboring subunit are shown in light blue.
18 Selected hydrogen bond interactions are shown in orange dotted lines.
19
20
21

22
23
24 **Figure 4.** Stereoview of the binding sites of *Hp*MTAN in complex with transition-state analogue inhibitors. The
25 inhibitor complexes of **15**, **16**, **30** and **32** are shown in panel A, B, C and D, respectively. The residues interacting
26 with inhibitors from monomer-A are shown in yellow and from monomer-B are shown in light blue. Selected
27 hydrogen bond interactions are shown in orange dotted lines.
28
29
30

31
32 **Figure 5.** Catalytic site conformations of apo- and ligand-bound MTAP and *Hp*MTAN. **(A)** Stereoview
33 superposition of unliganded MTAP (PDB ID: 3OZE; green) with four inhibitor-bound structures including MTAP-
34 **15** (PDB ID: 6DYZ; cyan), MTAP-**16** (PDB ID: 6DZ0; yellow), MTAP-**30** (PDB ID: 6DZ3; blue) and MTAP-**32**
35 (PDB ID: 6DZ2; light pink), are overlapped. The $\beta 1$ - $\beta 2$ loop (highlighted with red star) is altered substantially on
36 the binding of the **30** and **32**. **(B)** The superposition of an unliganded MTAN binding site (*E. coli* MTAN PDB ID:
37 1Z5P; blue) with four inhibitor bound complexes of *Hp*MTAN including MTAP-**15** (PDB ID: 6DYU; brick red),
38 MTAP-**16** (PDB ID: 6DYV; cyan), MTAP-**30** (6DYY; yellow) and MTAP-**32** (6DYW; red). The helix 6 and
39 associated loop of the unliganded MTAN changes conformation to elongate helix 6 as a result of inhibitor binding
40 (highlighted with a red star).
41
42
43
44
45
46
47
48
49
50
51
52
53
54
55
56
57
58
59
60

**Figure 1**

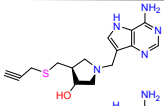
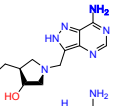
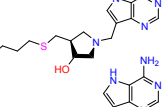
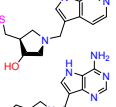
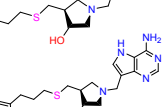
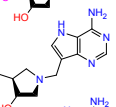
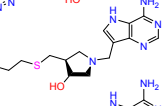
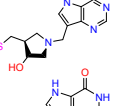
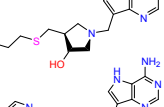
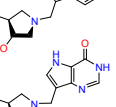
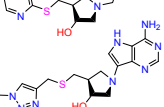
Code	Inhibitor	K_d (nM)			Code	Inhibitor	K_d (nM)		
		HsMTAP	HpMTAN	K_d Hs/Hp			HsMTAP	HpMTAN	K_d Hs/Hp
15		0.63 ± 0.08	0.055 ± 0.025	11.5	11		19 ± 1.5	0.235 ± 0.064	80.9
16		0.94 ± 0.12	0.026 ± 0.006	36.2	8		31.9 ± 7.9	10.3 ± 1.9	3.1
30		1.3 ± 0.1	0.028 ± 0.010	46.4	29		37 ± 7.0	0.373 ± 0.135	99.2
32		1.4 ± 0.1	0.036 ± 0.010	38.9	25		66 ± 6.6	0.274 ± 0.096	241
28		2.4 ± 0.3	0.026 ± 0.005	92.3	27		70 ± 3.2	0.288 ± 0.023	243
26		3.0 ± 0.2	0.025 ± 0.002	120	34		ND	ND	
33		13 ± 4.8	0.058 ± 0.006	224	35		ND	ND	
31		13 ± 1.4	0.073 ± 0.021	178					

Figure 2

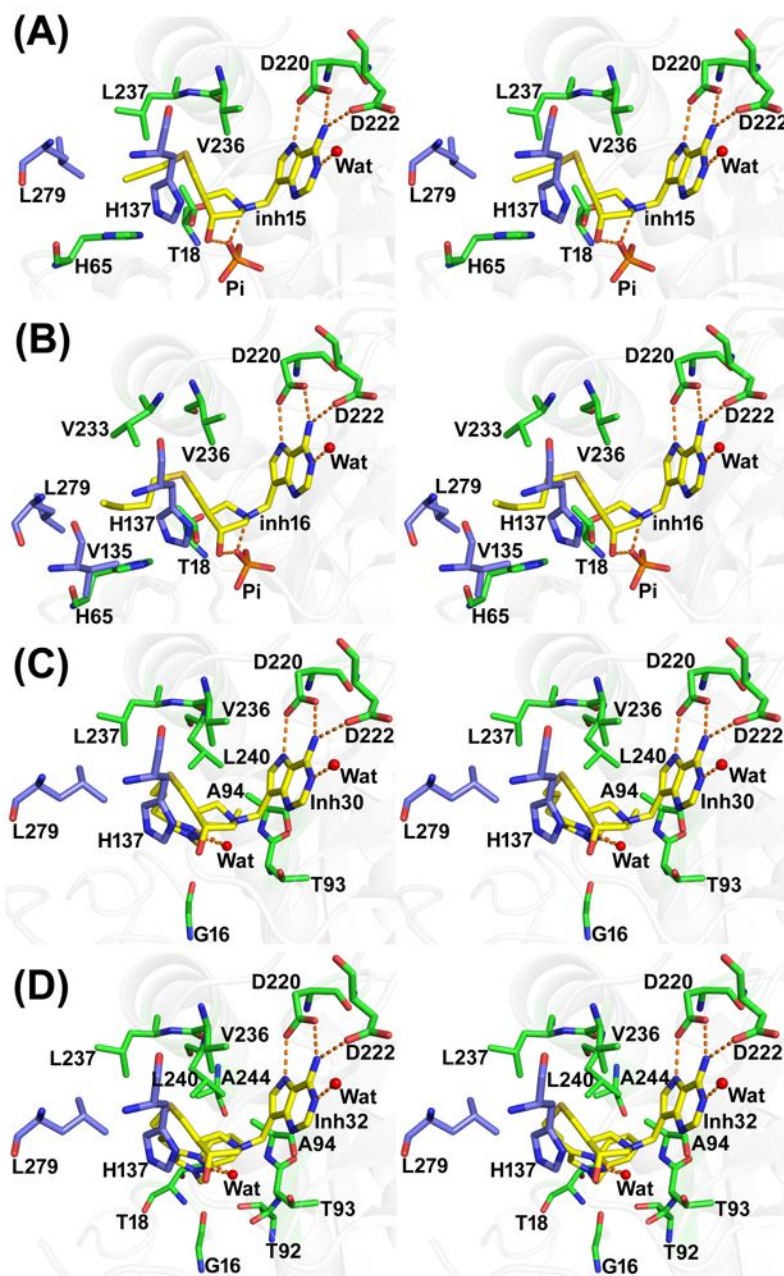


Figure 3

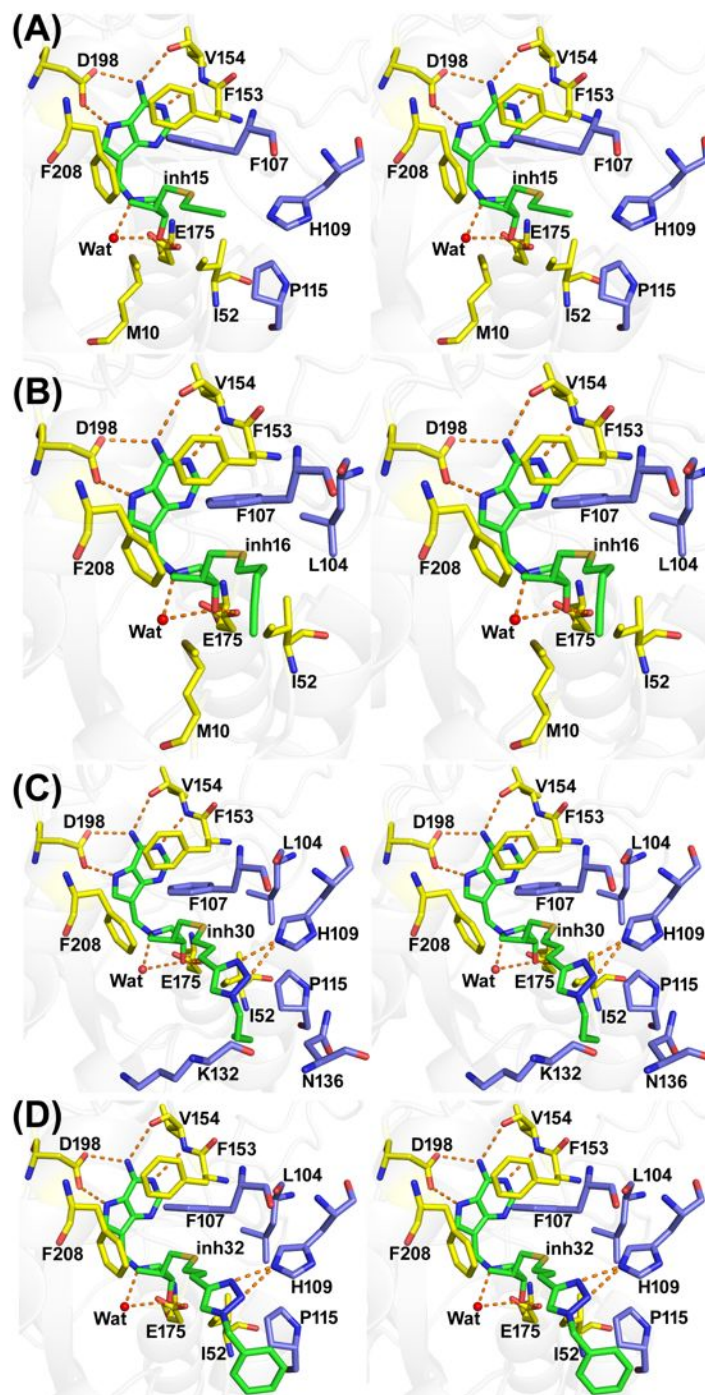


Figure 4

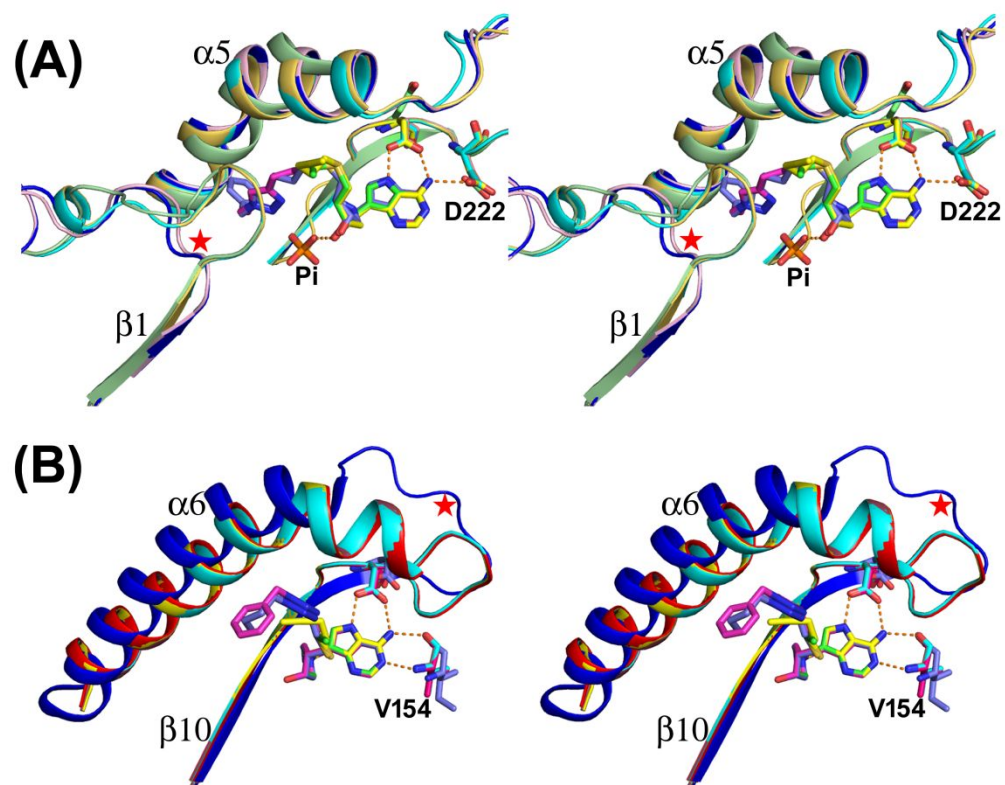


Figure 5

Table 1. Data collection and refinement statistics MTAP and HpMTAN complexes.

Dataset ^a	<i>H. sapiens</i> MTAP				<i>H. pylori</i> MTAN			
	MTAP + 15	MTAP + 16	MTAP + 30	MTAP + 32	HpMTAN + 15	HpMTAN + 16	HpMTAN + 30	HpMTAN + 32
Unit cell data								
Space group	P321	P321	C222 ₁	C222 ₁	P4 ₁ 2 ₁ 2	P4 ₁ 2 ₁ 2	P2 ₁ 2 ₁ 2 ₁	P4 ₁ 2 ₁ 2
Cell parameters (Å, °)	a = 122.82, b = 122.82, c = 44.62 α, β = 90 γ = 120.0	a = 121.81, b = 121.81, c = 44.37 α, β = 90 γ = 120	a = 79.36, b = 135.13, c = 158.86 α, β, γ = 90	a = 79.39, b = 135.32, c = 159.27 α, β, γ = 90	a = 73.25, b = 73.25, c = 176.14 α, β, γ = 90	a = 73.48, b = 73.48, c = 176.21 α, β, γ = 90	a = 72.56, b = 74.03, c = 176.89 α, β, γ = 90	a = 73.35, b = 73.35, c = 176.38 α, β, γ = 90
V _m (Å ³ /Dalton)	2.9	2.9	2.2	2.2	2.2	2.2	2.2	2.2
Number of subunits in the asymmetric unit	1	1	3	3	2	2	4	2
Data collection								
Beamline	LRL-CAT	LRL-CAT	LRL-CAT	LRL-CAT	LRL-CAT	LRL-CAT	LRL-CAT	LRL-CAT
Wavelength (Å)	0.97931	0.97931	0.97931	0.97931	0.97931	0.97931	0.97931	0.97931
Temperature (K)	100	100	100	100	100	100	100	100
Resolution range (Å)	53.18 – 1.62 (1.65 – 1.62)	60.91 – 1.62 (1.65 – 1.62)	79.43 – 1.91 (1.95 – 1.91)	79.63 – 1.99 (2.04 – 1.99)	67.64 – 1.60 (1.63 – 1.60)	88.10 – 1.62 (1.65 – 1.62)	176.89 – 1.61 (1.64 – 1.61)	88.19 – 1.45 (1.47 – 1.45)
Total number of observed reflections	605199 (28477)	600969 (27711)	497405 (33410)	438725 (30921)	927868 (45362)	852192 (25016)	912840 (44290)	1242406 (60058)
Number of unique reflections	48526 (2329)	48221 (2355)	66387 (4430)	59017 (4097)	64250 (3121)	61452 (2548)	123910 (5998)	86142 (4167)
R _{merge} (%) ^b	9.8 (121.8)	11.0 (133.5)	9.4 (109.3)	10.0 (116.2)	14.6 (152.8)	11.5 (109.4)	9.9 (99.1)	14.9 (175.4)
R _{pim} (%) ^c	2.9 (36.0)	3.2 (40.3)	3.7 (42.6)	3.9 (45.0)	4.0 (41.3)	3.1 (34.9)	3.9 (39.0)	4.1 (47.5)

CC1/2 (%)	99.9 (75.8)	99.9 (71.4)	99.8 (70.2)	99.9 (72.5)	99.9 (69.8)	99.8 (69.6)	99.7 (80.2)	99.7 (76.0)
< I/ σ (I)> ^d	18.3 (2.0)	14.9 (2.0)	13.0 (1.9)	13.4 (1.9)	13.8 (2.0)	14.8 (2.0)	11.4 (2.1)	11.2 (2.0)
Completeness (%)	98.6 (96.3)	100 (100)	99.9 (100)	99.9 (100)	100 (99.9)	98.7 (84.0)	100 (100)	100 (100)
Multiplicity	12.5 (12.2)	12.5 (11.8)	7.5 (7.5)	7.4 (7.5)	14.4 (14.5)	13.9 (9.8)	7.4 (7.4)	14.4 (14.4)
Wilson B-factor (Å ²)	15.5	15.5	27.2	35.2	15.1	14.7	16.7	13.2
Refinement								
R _{work} (%) ^e	16.9	15.5	19.7	20.1	16.4	16.7	18.0	17.7
R _{free} (%) ^f	19.0	17.6	22.2	23.6	19.3	19.3	20.3	20.0
No. of atoms	2444	2428	6758	6615	4208	4152	8152	4168
Protein atoms	2137	2132	6290	6199	3596	3587	7104	3568
Ligand atoms	22	24	93	102	44	48	124	68
Solvent atoms	285	272	375	314	568	517	924	532
Model quality								
RMS deviation from ideal value								
Bond length (Å)	0.011	0.011	0.009	0.01	0.01	0.01	0.01	0.009
Bond angle (°)	1.6	1.6	1.6	1.6	1.5	1.6	1.7	1.6
Average B-factor								
Protein atoms (Å ²)	21.6	22.3	38.3	43.8	17.7	20.6	23.3	18.8
Ligand atoms (Å ²)	16.4	17.3	41.0	46.1	13.3	15.5	23.1	21.0
Waters (Å ²)	36.1	36.5	40.1	42.1	31.5	33.3	34.5	31.5
Ramachandran plot^g								
Most favored regions (%)	97.5	98.2	97.7	98.0	97.1	96.9	97.0	96.6
Allowed regions (%)	2.5	1.8	1.7	2.0	2.9	3.1	3.0	3.4
Outlier regions (%)	0.0	0.0	0.6	0.0	0.0	0.0	0.0	0.0
PDB ID entry	6DYZ	6DZ0	6DZ3	6DZ2	6DYU	6DYV	6DYY	6DYW

^aValues in parentheses refer to the highest resolution shell.

^b $R_{\text{merge}} = (\sum_{\text{hkl}} \sum_i |I_i(\text{hkl}) - \langle I(\text{hkl}) \rangle|) / \sum_{\text{hkl}} \sum_i \langle I_i(\text{hkl}) \rangle$, where $I_i(\text{hkl})$ is the intensity of the i^{th} measurement of reflection (hkl) and $\langle I(\text{hkl}) \rangle$ is its mean intensity.

^c $R_{\text{pim}} = (\sum_{\text{hkl}} [1/(N_{\text{hkl}}-1)]^{1/2} \sum_i |I_i(\text{hkl}) - \langle I(\text{hkl}) \rangle|) / \sum_{\text{hkl}} \sum_i \langle I_i(\text{hkl}) \rangle$, where $I_i(\text{hkl})$ is the intensity of the i^{th} measurement of reflection (hkl), $\langle I(\text{hkl}) \rangle$ is its mean intensity and N is the number of measurements.

^d I is the integrated intensity and $\sigma(I)$ is its estimated standard deviation.

^e $R_{\text{work}} = (\sum_{\text{hkl}} |F_o - F_c|) / \sum_{\text{hkl}} F_o$ where F_o and F_c are the observed and calculated structure factors.

^f R_{free} is calculated as for R_{work} but from a randomly selected subset of the data (5%), which were excluded from the refinement calculation.

^gCalculated by MOLPROBITY.

Table 2: Amino acid residues in contact with the 5'-alkylthio groups of transition-state analogue inhibitors. Amino acids interacting within the 5'-alkylthio pocket (to 3.9 Å) are reported. Those residues interacting from the neighboring subunits are highlighted with an asterisk (*).

Inhibitors	MTAP	<i>Hp</i> MTAN
15	Thr18, His65, Val236, Leu237, His137*, Leu279*	Met10, Ile52, Phe153, Phe208, Phe107*, His109*, Pro115*
16	Thr18, His65, Val233, Val236, Val135*, His137*, Leu279*	Met10, Ile52, Phe153, Phe208, Leu104*, Phe107*
30	Gly16, Thr93, Ala94, Val236, Leu237, Leu240, His137*, Leu279*	Ile52, Phe153, Phe208, Leu104*, Phe107*, His109*, Pro115*, Lys132*, Asn136*
32	Gly16, Thr18, Thr92, Thr93, Ala94, Val236, Leu237, Leu240, Ala244, His137*, Leu279*	Ile52, Phe153, Phe208, Leu104*, Phe107*, His109*, Pro115*

Table of Content Graphics

